

Metasurfaces for neutral-atom trapping

Chengyu Fang¹, Minjeong Kim¹, Mark Saffman^{2,3}, Jennifer T. Choy^{1,2}, and Mikhail A. Kats^{1,2,*}

¹Department of Electrical and Computer Engineering, University of Wisconsin-Madison, 1415 Engineering Drive, Madison, WI 53706, USA

²Department of Physics, University of Wisconsin-Madison, 1150 University Avenue, Madison, WI 53706, USA

³Inflection, Madison, WI 53703, USA

*Corresponding author: mkats@wisc.edu

Abstract

Trapped neutral atoms are one of the leading platforms for quantum information technologies, in particular for quantum computing, but scaling them to array sizes needed for utility-scale quantum computing is a major engineering challenge. Here we review optical metasurfaces as an enabling technology that provides fine control over the phase, amplitude, and polarization of light, with pixel counts far exceeding what is available with spatial light modulators (SLMs) and other active devices. The large pixel counts have recently led to demonstrations of arrays of optical tweezers with hundreds of thousands of sites and arrays of optical bottle-beams with complex three-dimensional trapping profiles. The flexibility and scalability of optical metasurfaces provides a route towards miniaturized, integrated, and highly scalable atomic experiments and instruments.

1 Introduction

Neutral-atom arrays are enabling components for a class of quantum computers, and for quantum networking and sensing [1]. The primary existing approach to trap arrays of atoms involves the use of active optical devices, such as spatial light modulators (SLMs) [2–5], digital micromirror devices (DMDs) [6, 7], and acousto-optic deflectors (AODs) [8–10] to form arrays of optical dipole traps. These active devices can generate dipole-trap arrays with thousands of sites [5], enable atom rearrangement to form defect-free arrays [3], and facilitate coherent transport between sites for non-local connectivity [10, 11].

Despite the flexibility offered by active optical devices, further scaling and integration of neutral-atom arrays face several engineering challenges. For example, the pixel count of SLMs and DMDs limits the number of traps a single device can generate, and a similar limitation exists in AODs related to the radio-frequency bandwidth. It is possible to use multiple active devices simultaneously to get around, e.g., the pixel limitations of SLMs [5, 12], but the integration is complex, and so far the number of traps generated via SLMs (up to 12,000 sites [5]) falls short of the predicted number of qubits needed to achieve quantum advantage in factoring integers [13, 14] or quantum chemistry problems [15, 16]. We note that a recent work argues that the requirement could be brought down to as few as $\sim 10,000$ reconfigurable atomic qubits for Shor’s algorithm [17], albeit with runtimes ranging from months to over a century at that qubit count; practical runtimes of days to months still require roughly an order of magnitude more physical qubits.

The limitations of active optical devices for atom trapping have motivated the design of trap arrays using passive optical elements, including micro-lens arrays (MLAs) [18–22] and re-imaged optical intensity masks [23, 24]. These passive components can be manufactured to large scales, potentially enabling very large atom arrays. However, both of these technologies need extra optics to deliver and de-magnify the beams into the vacuum cell, hindering integration and miniaturization. These approaches also have limited functionality; for example, MLAs are not able to easily form complex beams such as optical bottles.

Here we review an emerging approach to creating large arrays of optical traps, using optical metasurfaces manufactured using semiconductor fabrication techniques. Metasurfaces are flat optical components that provide subwavelength control of optical wavefronts, and can replace combinations of active and passive optical components [25]. We discuss how metasurfaces may enable (i) the scaling of optical-tweezer arrays to millions of sites, (ii) the generation of complex trapping profiles like optical bottle beams, (iii) multiple functionalities like polarization multiplexing or trapping and imaging in a single optic. We also discuss practical aspects and challenges of metasurface design, including material choices, miniaturization, and integration into complex optical and vacuum systems.

2 Array scalability

Scalability of trapped-atom arrays is essential for advancing quantum technologies, especially for quantum computing. In a Rydberg-atom-based quantum computer (Fig. 1(a)), each trapped atom stores quantum information in two electronic states, which are hyperfine ground states for alkali atoms such as Rb and Cs, or nuclear-spin states for alkaline-earth(-like) atoms such as Sr and Yb [1]. Neighboring atoms can be entangled after being excited to Rydberg states [26]. Quantum gate operations are then implemented with sequences of laser or microwave pulses applied either globally to the array or to individual atoms. Solving complex quantum chemistry problems, such as ground-state energy estimation of iron-molybdenum cofactor (FeMoco), requires millions of physical qubits [16], because thousands of logical qubits are required and each logical qubit may require up to thousands of physical qubits [14].

Here, we compare the experimentally demonstrated active and passive optical devices to generate tweezer arrays (Table 1). We focus on how each approach scales with the number of trap sites, and what (if anything) will limit further scalability. SLMs used in atom-trapping experiments are typically liquid-crystal phase-only panels that apply a pixel-by-pixel $0-2\pi$ phase profile to the incident laser beam; then a high numerical aperture (NA) lens focuses the resulting wavefront into the vacuum cell. The phase profile at the SLM is typically calculated using the Gerchberg-Saxton (G-S) algorithm [31] or its variants [29, 32], to achieve some target trapping profile. This phase-only (holographic) approach redistributes the energy of light in a reasonably power-efficient manner, especially for sparse arrays, with typical first-order diffraction efficiency of 40 – 60% [3, 33] (meaning about half of the light is lost). Due to the relatively slow response of liquid crystals (typically tens to hundreds of Hz), SLMs are primarily used for generating static traps, although rearrangement to achieve defect-free arrays using SLMs has also been demonstrated [3, 34].

Until very recently, the largest experimentally demonstrated atom array [5] used two 1024×1024 SLMs in parallel to achieve one complete array with $\sim 12,000$ trapping sites, stochastically loaded with $\sim 6,100$ atoms (Fig. 1(b)). To further scale the number of traps toward the million-site level, the SLM approach faces a bottleneck in the pixel budget. With a typical ratio of ~ 300 pixels per trap [27], a million-site array would require hundreds of millions of pixels, which are orders of magnitude beyond the available pixel counts in commercial SLMs. The gap is even larger for the

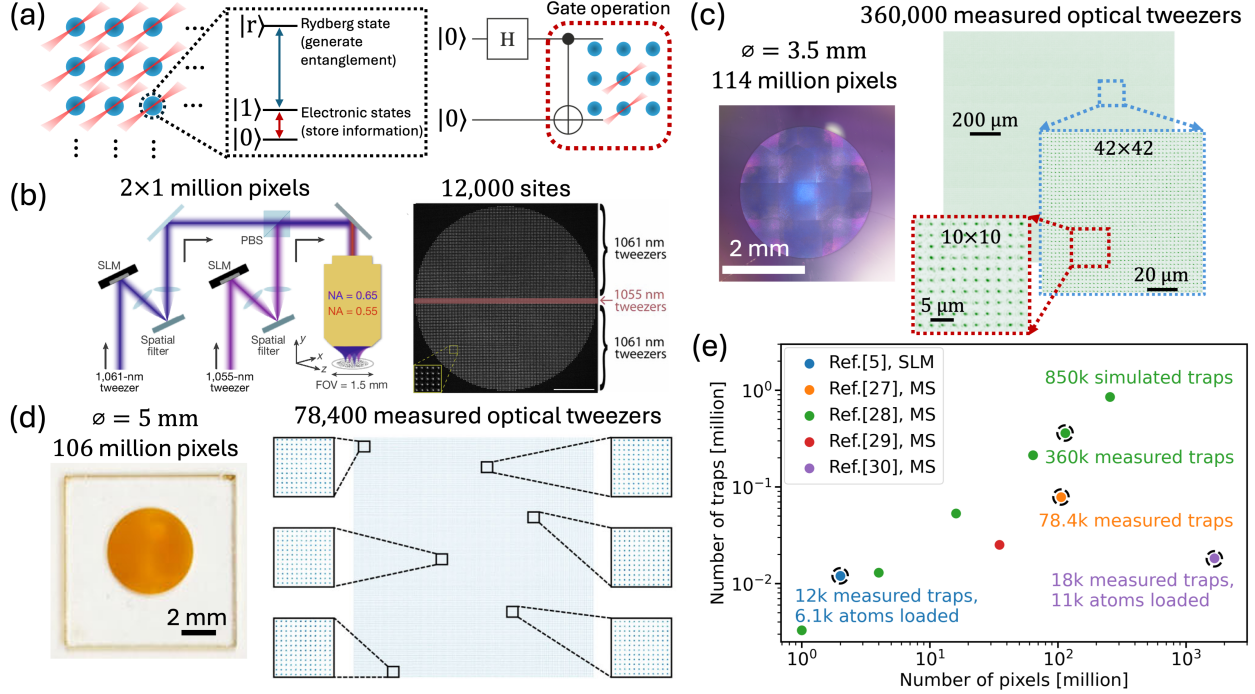


Figure 1: Approaches to scale neutral-atom tweezer arrays. (a) Schematic of a neutral-atom quantum computer, where atoms are trapped in an optical-tweezer array, with qubits encoded in two electronic states ($|0\rangle$ and $|1\rangle$). A Rydberg state ($|r\rangle$) enables entanglement between neighboring atoms, enabling multi-qubit gates such as the CNOT shown on the right. (b) An array of 12,000 tweezer sites generated by two 1024×1024 SLMs (~ 2 million pixels in total) using 1061 nm and 1055 nm laser, with 6,100 atoms loaded; adapted from [5]. (c) An array of 360,000 tweezer sites generated by a 3.5-mm-diameter metasurface with 114 million pixels (no atoms loaded in the device shown, although single-atom trapping was demonstrated in a smaller array reported in this work); representing the results in [27]. (d) An array of 78,400 tweezer sites generated by a single 5-mm-diameter metasurface with 106 million pixels (no atoms loaded); adapted from [28]. (e) Summary of literature on metasurfaces for atom trapping [27–30], with the number of tweezers formed as a function of the number of metasurface pixels. For reference, the record result using two SLMs is also included [5]. Dashed circles mark experimentally demonstrated metasurfaces; the remaining data points correspond to simulated designs. “Measured traps” means the traps were imaged, but atoms may not have been loaded.

high-power variants of SLMs, which offer fewer pixels due to tighter thermal constraints, but are often required because trapping a single atom typically requires mW-level laser power, which scales to hundreds of watts for a large array. As an example, Ref. [5] uses total laser power exceeding 100 watts. SLMs also generally have lower diffraction efficiency when illuminated by high-power lasers due to the degradation of performance in the liquid crystals [35], which further hinders the scalability.

The DMD, another pixelated optical device, imprints a binary amplitude mask on the beam, with grayscale amplitude produced by kilohertz (kHz) pulse-width modulation (PWM) on each micro-mirror. The beam profile can then be re-imaged into the vacuum cell to trap atoms. Because DMDs act as amplitude masks, they are less power-efficient than phase SLMs for sparse tweezer arrays [36], and their PWM modulation can drive parametric heating when it overlaps with the

atom trapping frequencies [6]. Due to these limitations, DMDs are not commonly used for single-atom array generation.

AODs deflect the incident beam through Bragg diffraction from an acoustic wave in a crystal driven by radio-frequency (RF) tones, where applying multiple tones simultaneously can generate several beams at different angles, followed by focusing to generate a one-dimensional array of traps. A two-dimensional array can be generated by two orthogonally positioned AODs. AODs operate at megahertz (MHz) rates which enables fast movement of single atoms [8, 9]. However, the number of independently addressable beams is set by the RF bandwidth divided by the minimum RF tone spacing, typically limiting a single AOD to tens of beams. So, AODs are best suited for fast reconfiguration instead of generating large static arrays. These complementary trade-offs to SLMs motivate the hybrid architecture of using SLMs for generating large static arrays and AODs for fast rearrangement of atoms between sites [5, 10].

Active devices provide the capabilities to rearrange atoms [4, 8, 34] and improve the uniformity by using real-time feedback [37]. However, they face significant engineering challenges to scale to much larger atom numbers. SLMs are the leading platform to generate large-scale trap arrays, but they still do not provide a clear path to scale to millions of trap sites. A solution is passive optical components that are simpler to design and fabricate than a complete SLM, and can thus be easily scaled. For example, a laser beam incident on a passive optical intensity mask, e.g., an array of apertures, can be turned into an array of optical traps via re-imaging of the mask surface into a vacuum cell. Binary [23] and ternary [24] intensity masks are straightforward to make up to arbitrary sizes using conventional fabrication processes, and spatial filtering in the Fourier plane can yield high-quality optical traps. Amplitude masks have been used to demonstrate arrays of tweezer beams, bottle beams, and interleaved arrays that can trap individual atoms of two species using a single laser [24]. Because the re-imaging optics can be designed to have various demagnifications, the feature size on the mask can be relatively large and easily achievable by even low-resolution lithography, which makes fabrication easy and readily scalable. However, similarly to DMDs, the trapping approach using amplitude optical masks has limited power efficiency, especially for sparse tweezer arrays, where a large fraction of light ends up reflected or absorbed at the mask.

A micro-lens array (MLA) is another type of passive optic that can generate traps when illuminated by a trapping laser [18–22], with pitch sizes ranging from tens to hundreds of microns. Each micro-lens focuses the incident light into a spot, and this spot can be de-magnified and re-imaged into the vacuum cell for atom trapping. MLA-based tweezer arrays have been scaled to $\sim 3,000$ sites [22]. However, further scaling is limited by several factors: the size of each micro-lens limits the number of lenses that fit within a reasonable optical aperture of the imaging system, and the dead area between neighboring micro-lenses limits the power efficiency.

Perhaps the most flexible passive optical components are optical metasurfaces, which are planar optical elements that provide subwavelength control over the phase, amplitude, and/or polarization of light passing through them. Metasurfaces can serve a similar role to SLMs, generating arbitrary field profiles holographically, but they have much smaller pixels (i.e., metasurface unit cells), suppressing higher-order diffraction that limits efficiency in SLMs, and can be scaled to nearly arbitrary pixel counts, which are only limited by the writing time of high-resolution lithography. Two studies demonstrated the scaling opportunities offered by metasurfaces, with Holman et al. generating 360,000 tweezer sites using a 3.5-mm-diameter metasurface containing 114 million titanium-dioxide meta-atoms (Fig. 1(c)) [27], and Wang et al. demonstrating tweezer arrays with 78,400 sites using a 5-mm-diameter metasurface containing 106 million silicon-nitride meta-atoms (Fig. 1(d)) [28]. Very recently, a single 19.8-mm-diameter metasurface with about 1.7 billion silicon-nitride meta-atoms trapped about 11,000 atoms in an 18,225-site array [30], exceeding the largest atom number reported with SLMs [5]. Figure 1(e) shows that the number of traps can scale roughly linearly

Table 1: Comparison of optical devices for generating tweezer arrays

Device	Refresh rate	Largest number of optical traps demonstrated	Largest number of single atoms loaded
SLM	sub kHz	$\sim 12,000$ sites [5]	$\sim 6,100$ atoms [5]
DMD	\sim kHz	20 sites [6]	~ 2 atoms [6]
AOD	\sim MHz	512 sites [12]	~ 270 atoms [12]
Amplitude mask	static	1,225 sites [23]	~ 370 atoms [23]
MLA	static	$\sim 3,000$ sites [22]	~ 1167 atoms [22]
Metasurface	static	360,000 sites [27]	$\sim 11,000$ atoms [30]

with pixel count, with the slope set by factors such as the target array uniformity [27]. We note that the metasurface in Ref. [30] has 1.7 billion pixels which far exceeds what is needed for the demonstrated 18,225 traps; in that work, the larger pixel number was used to enlarge the aperture to create a longer working distance, enabling the metasurface positioned outside of the vacuum cell to generate traps inside the cell.

Beyond the current demonstrations, the pixel budget of a single metasurface has a path to scale to much larger sizes. In most laboratory demonstrations, metasurfaces are patterned using electron-beam lithography [27–29, 38–40], which is a serial technique and thus limits the achievable pixel counts. However, other lithography methods, e.g., deep-ultraviolet [41] and nanoimprint [42] lithography, can be used to dramatically improve the scalability and throughput. As an example, an all-glass 100-mm-diameter visible metalens with 18.7 billion pixels has been demonstrated [41], which is one order of magnitude larger than the largest metasurface fabricated for atom trapping [30].

3 Bottle-beam generation

The large pixel count of metasurfaces enables more sophisticated amplitude and phase control of a beam, enabling complex three-dimensional traps. In this section, we focus on arrays of optical bottle beams, which have a dark “focal spot” surrounded by a bright shell. Optical bottle beams can trap atoms at the intensity-null center when the laser is blue-detuned from the atomic transition. Bottle beams are more difficult to form than tweezers because they have a broader Fourier spectrum [43], and significantly better phase control in the plane of traps is required to form a complete three-dimensional bottle, requiring more metasurface pixels.

Despite the added complexity, optical bottles offer several advantages for neutral-atom applications, especially computing [26]. First, trapping atoms at an intensity null rather than at intensity maximum reduces photon scattering from the trap light, supporting longer trap lifetimes and coherence times [44–47]. Also, atoms in bottle beams are less sensitive to trapping-laser intensity fluctuations because the light intensity at the atom position is small, so the same fractional fluctuation produces a smaller perturbation compared to optical tweezers. Finally, bottle beams avoid workarounds needed because the AC polarizability of alkali atoms flips sign between ground and

Rydberg states at typical tweezer wavelengths [48], which results in anti-trapping of atoms in a tweezer during Rydberg excitation. Existing workarounds include using near-resonance trapping wavelengths that avoid anti-trapping but increase photon scattering [48, 49], or switching off the trap during Rydberg excitation and recapturing the atom afterward [50], which can cause atom loss and motional heating [51–53]. In a blue-detuned bottle beam, atoms remain confined during Rydberg excitation [54], and a “magic” wavelength can further be chosen at which the polarizability is the same for ground and Rydberg states, eliminating differential light shifts [55].

Several approaches have been demonstrated to form a single bottle beam. A bottle beam can be created via destructive interference between two Gaussian beams with slightly different waists (Fig. 2(a) [56]), or using a phase-only SLM [54]. Single bottle beams have also been demonstrated using metasurfaces [57, 58]. For example, as shown in Fig. 2(b), a single passive metasurface illuminated by a Gaussian beam can generate a bottle-beam trap at the focal plane with higher efficiency compared to a two-beam interference approach. A polarization-multiplexed metasurface has also been used to generate a bottle beam (Fig. 2(c) [58]), with the polarization multiplexing functionality discussed in the following section.

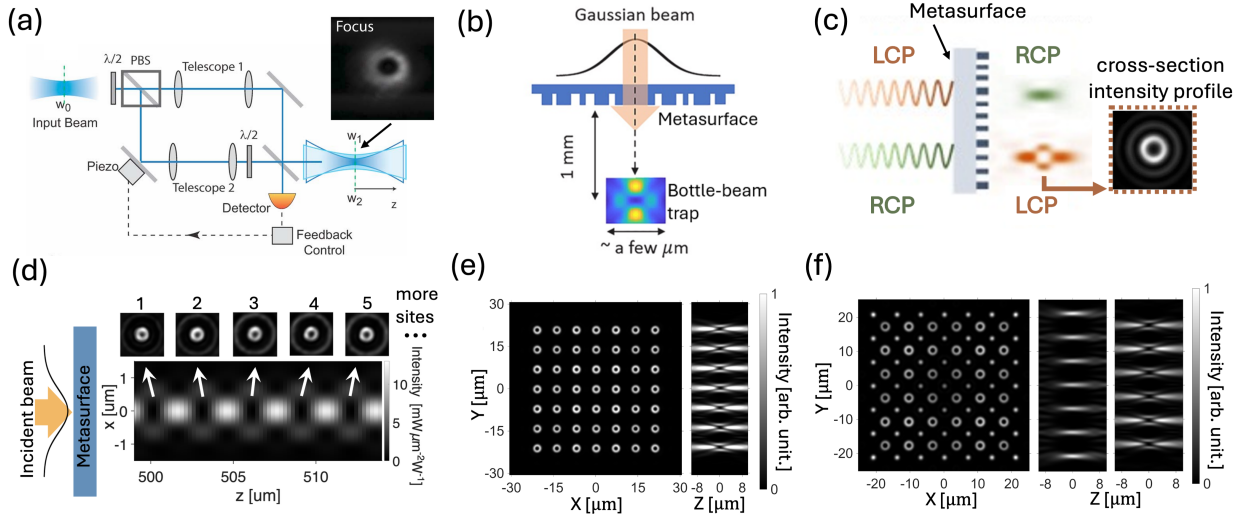


Figure 2: Generation of optical bottle beams. (a) Bottle-beam trap generated by destructive interference of two co-propagating Gaussian beams with different waists, stabilized by an active phase lock; adapted from [56]. (b) Single dark trap generated from an incident Gaussian beam by a ~ 1 -mm metasurface, optimized for high efficiency and trap quality; adapted from [57]. (c) Polarization-multiplexed metasurface that generates a bright trap for one circular polarization and a dark trap for the opposite circular polarization; adapted from [58]. (d) One-dimensional array of ten dark traps generated by a metasurface; five of the sites are shown in X-Z and Y-Z, for the optic axis along Z; adapted from [59]. (e) Two-dimensional 7×7 dark-trap array generated by a single metasurface, shown in X-Y (in the focal plane; left) and in X-Z (right) along the trap centers; adapted from [29]. (f) Two-dimensional array of interleaved 7×7 bright traps and 6×6 dark-trap arrays generated by a single metasurface, shown X-Y (left) and X-Z along the bright array (middle), and along the dark array (right); adapted from [29].

Bottle beams are more difficult to form than optical tweezers because they require simultaneous control over both amplitude and phase in the focal plane to form the traps in three dimensions [29]. This added degree of freedom compared to optical tweezers demands more pixels when the wavefront

is generated holographically using SLMs or metasurfaces. For this reason, to our knowledge, there have not been demonstrations of large arrays of bottle beams using an SLM. Metasurfaces, which can provide orders-of-magnitude more pixels than SLMs (Section 2), are therefore a natural route to large, high-quality bottle-beam arrays.

A one-dimensional array of ten optical bottles was recently implemented using a metasurface with TiO_2 meta-atoms, where each optical bottle is formed along the optic axis at locations of point phase singularities (Fig. 2(d)) [59]. A two-dimensional array of bottle beams was demonstrated using a silicon-on-sapphire metasurface, where the array was in a single focal plane (Fig. 2(e) [29]), which is the atom geometry most commonly used in neutral-atom quantum computing using SLMs. In Ref. [29], the conventional G-S algorithm for designing the phase profile on the metasurface was insufficient because it does not enforce a particular phase profile in the focal plane, and a modified G-S algorithm that enforces both amplitude and phase near the trapping sites (but leaves the field unconstrained elsewhere) was developed instead.

The modified G-S approach was also used to design metasurfaces that generate arrays in which bright and dark traps are spatially interleaved (Fig. 2(f) [29]). By selecting a trapping wavelength at which two atomic species have polarizabilities of opposite signs, a single laser can be used to trap one atomic species in the bright trap, and the other in the dark trap, which can be advantageous for quantum error correction [60]. More complicated two-dimensional geometries, such as interleaved dual-species pentagonal lattices [61], can also be readily generated using metasurfaces.

4 Multi-functionality, miniaturization, and integration

Beyond the optics used to generate trap arrays, the complexity of neutral-atom hardware also includes vacuum components, infrastructure to cool atomic ensembles, and optics for fluorescence readout. These functions require many optical components, including non-standard ones modified for working with vacuum cells, such as specialized objectives for imaging through thick glass walls [62], and anti-reflection coatings for high-NA optics. Each additional optical component introduces alignment degrees of freedom and can contribute to wavefront distortion and power loss. This becomes increasingly more difficult to manage for systems that need to either scale or to be compact and portable.

The metasurface approach can help reduce the number of distinct optical components. Because each meta-atom can be designed to have different responses as a function of wavelength and polarization, a single metasurface can perform multiple optical functions. In this section, we show how multi-functional metasurfaces are becoming incorporated in atom-trapping experiments, and how they can enable more-integrated atomic instruments.

Before single atoms can be trapped in tweezer or bottle-beam traps, a cloud of atoms must be localized and cooled using a magneto-optical trap (MOT) [63], which conventionally uses three pairs of counter-propagating circularly polarized beams with controlled handedness. This typically requires multiple waveplates, polarizing beam splitters, and mirrors (often retroreflectors), with demanding alignments. Multi-functional metasurfaces provide a path to reduce the number of optics in a MOT. For example, Fig. 3(a) shows a metasurface that splits one circular-polarized beam into five output beams with uniform power ratios and circular polarizations, enabling a compact MOT [64]. The beam-splitting function was achieved by using a gradient phase profile, while the wave-plate function was enabled by birefringent meta-atoms at each pixel. Building on this platform, Ref. [65] used a second metasurface to replace the wave plate and the mirror that remained in Fig. 3(a), further reducing the number of optics.

In addition to magneto-optical trapping and then dipole trapping of single atoms, atomic ex-

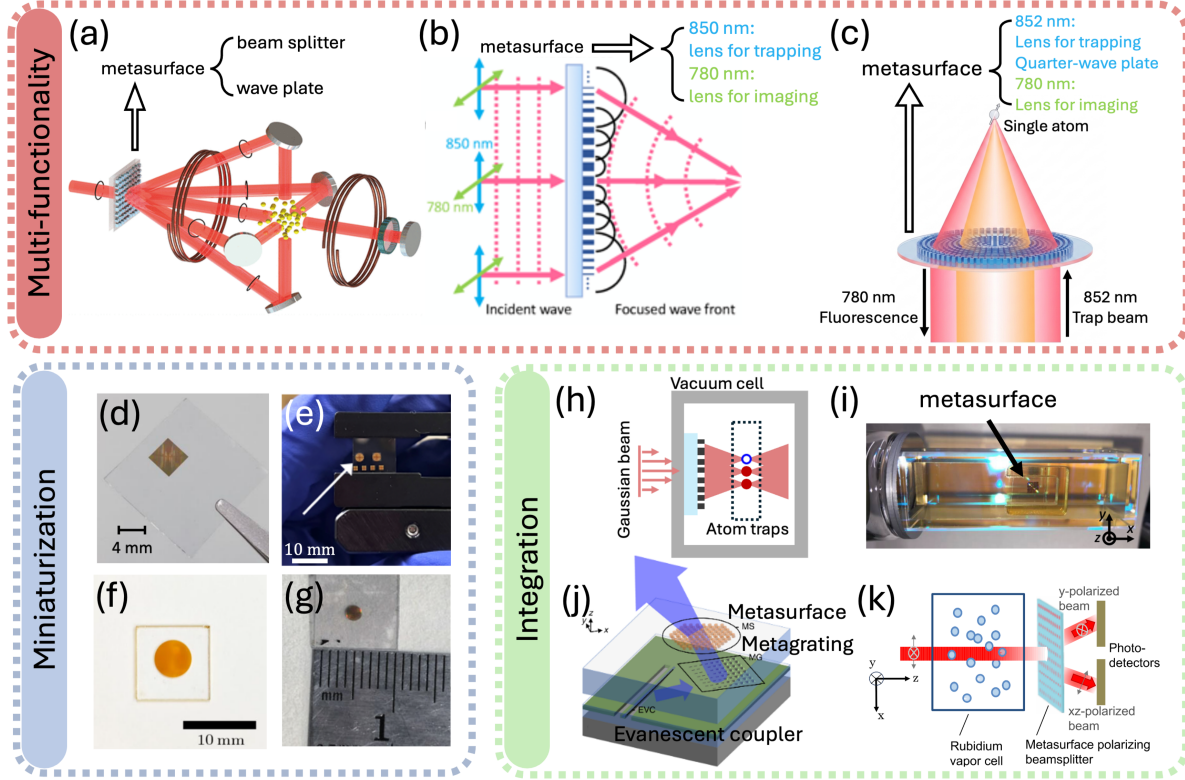


Figure 3: Multi-functionality, miniaturization, and integration enabled by metasurfaces in atom-trapping optical systems. (a) Multi-functional metasurface for generating a MOT, combining beam splitting and polarization control to generate five cooling beams from one incident beam; adapted from [64]. (b) Polarization-multiplexed metalens, operating for two wavelengths (780 nm and 850 nm) for two orthogonal linear polarizations; adapted from [38]. (c) Wavelength-multiplexed metalens at 780 nm and 852 nm, which adds quarter-wave-plate functionality only at 852 nm; adapted from [66]. (d–g) Representative compact metasurfaces that range from sub-millimeter to a few millimeters; adapted from [28, 29, 38, 66]. (h) Schematic of bright- and dark-trap generation using a metasurface integrated inside a vacuum cell; adapted from [29]. (i) An amorphous silicon on fused silica metasurface integrated inside a vacuum glass cell to replace high-NA objective; adapted from [38]. (j) Integrated metasurface platform to launch a centimeter-scale circularly polarized beam for generating MOTs; adapted from [67]. (k) Metasurface integrated to a rubidium-vapor atomic magnetometer for balanced polarimetry in a rubidium-vapor atomic magnetometer; adapted from [68].

periments need readout optics, achieved using fluorescence imaging [1]. The imaging and trapping optical paths usually share one high-NA objective, but are then split using a dichroic into the trapping path (into the cell) and a path for fluorescence imaging (out of the cell, at the resonance wavelength of the atoms) leading to a single-photon camera. Metasurfaces can in principle streamline these optical systems, with initial demonstrations including a polarization-multiplexed metalens, with one polarization for the trapping wavelength and another for the imaging wavelength (Fig. 3(b)) [38], and a wavelength-multiplexed metalens which builds in a wave-plate functionality at only the trapping wavelength (Fig. 3(c)) [66]. In both of these demonstrations, efficiency remains a challenge because the multi-functionality was enabled by polarization multiplexing [38] or spatial interleaving [66], although potentially higher-efficiency achromatic designs can be achieved

by engineering the dispersion of each meta-atom [69].

While providing multi-functionality, metasurfaces remain compact for two reasons. First, each meta-atom has subwavelength dimensions (hundreds of nanometers) [25] instead of several to tens of micrometers per pixel in phase SLMs. Second, because they are passive, metasurfaces do not need the electronics and cooling hardware that surrounds SLM panels. This size difference allows a millimeter-scale metasurface to contain 10^7 – 10^8 independently patterned pixels [28, 29, 38, 66], which is one to two orders of magnitude more than that of a bulky SLM.

Their compact size makes metasurfaces easier to integrate with other atom-trapping hardware, like vacuum cells. As proposed in Ref. [29], a metasurface can be put directly into the vacuum cell (Fig. 3(h)), which can reduce the wavefront distortion introduced by the cell wall [70], and remove the need for sophisticated objectives that compensate for the wall thickness. The integration is possible because most metasurfaces comprise dielectrics and semiconductors which can tolerate the vacuum bake-out [71] to achieve high vacuum. Integration of metasurfaces inside vacuum cells was experimentally realized in Ref. [38], where the metasurface is bonded to the vacuum cell using epoxy that survives the baking cycle (Fig. 3(i)).

Metasurfaces can also be integrated with photonic integrated circuits (PICs) and optical fibers, which can generate and deliver laser light without bulky free-space optics [72–76], with the metasurfaces providing additional control over the angle, size, and polarization of outcoupled beams. For example, metasurfaces have been used to set the angles, sizes, and circular polarizations of twelve MOT beams for laser cooling of strontium at 461 nm and 689 nm, together with co-propagating 813-nm lattice and 698-nm clock beams [67] (Fig. 3(j)). Without the metasurfaces, each port would require its own stack of optics, which is difficult to scale across multiple wavelengths and tens of ports on one chip. Beyond cold-atom systems, metasurfaces can also enable integration of quantum sensors based on vapor cells, such as atomic magnetometers [77, 78] that need to be as small as possible for field deployment [79–81]. For example, Yang et al. integrated a silicon-on-sapphire metasurface polarizing beam splitter with a rubidium vapor cell for balanced polarimetry, replacing a conventional Wollaston prism with a single planar element [68] (Fig. 3(k)).

5 Materials and fabrication

A material platform for atom-trapping metasurfaces needs to provide both sufficient phase control and low optical loss at the operating wavelength. A higher refractive index (n) helps achieve full 0 – 2π phase coverage at low-to-moderate aspect ratios of meta-atoms [82], simplifying fabrication, but a high n is only useful when the extinction coefficient (κ) is sufficiently small at and around the relevant visible and near-infrared (NIR) atomic transitions.

Fig. 4(a) shows the refractive index of several materials that have been used for metasurfaces, along with their low-loss wavelength ranges, here defined as $\kappa < 0.01$. Due to metasurfaces being thin (i.e., the height of meta-atoms is typically hundreds of nanometers), they can tolerate significantly higher material losses than would be feasible for thick windows or for photonic integrated circuits. In some cases, the loss tolerance of metasurfaces enables the use of semiconductors for photon energy above their band gaps; for example, crystalline silicon (c-Si) can be used for wavelengths as short as 650 nm due to its indirect band gap (Fig. 4(a)). In general, there is a tradeoff between high refractive index and broader transparency window due to the inverse relationship between band gap and refractive index [83], so materials that are transparent across the entire visible and near-infrared ranges have indices no higher than ~ 2.5 . TiO_2 and Si have been widely used for metasurfaces [84–87], including for atom trapping [29, 38, 39, 66], though other material choices may be preferable when weighing refractive index and losses at the wavelength of interest,

material and substrate availability, and fabrication complexity.

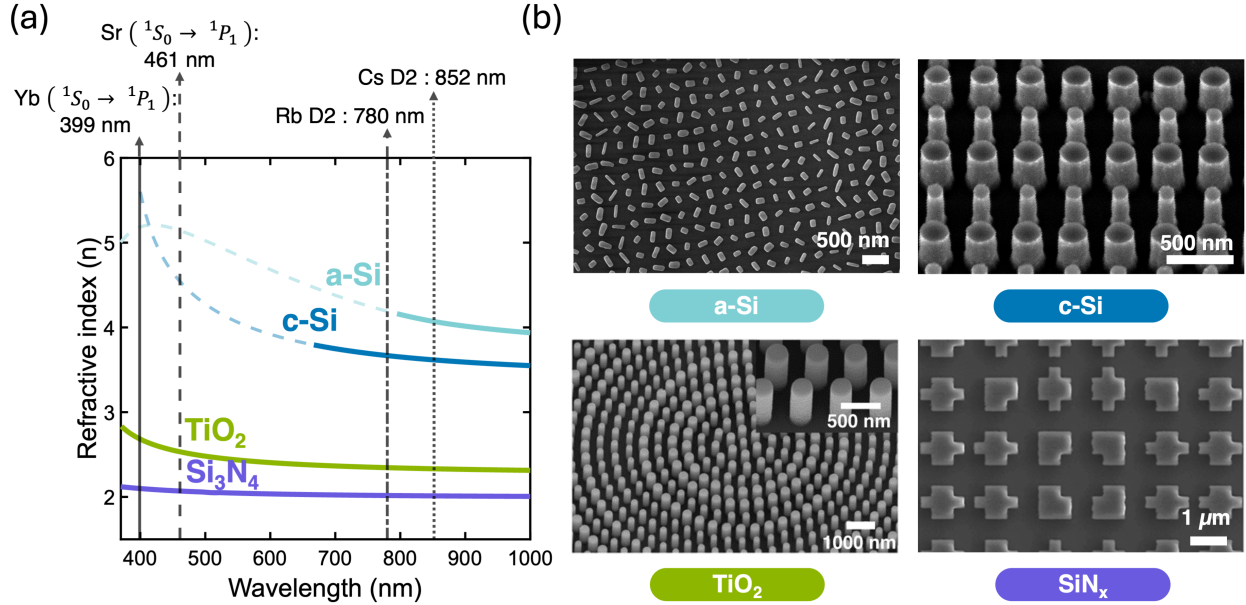


Figure 4: Optical materials for neutral-atom trapping metasurfaces (a) Refractive index (n) as a function of wavelength for metasurface materials, including a-Si [88], c-Si [29], TiO₂ [82], Si₃N₄ [89]. Solid curves indicate low-loss regions with $\kappa < 0.01$, while dashed curves indicate absorbing regions with a larger extinction coefficient. Vertical dashed lines mark several representative atomic transitions: Yb at 399 nm, Sr at 461 nm, Rb D2 at 780 nm, Cs D2 at 852 nm. (b) Scanning electron microscope (SEM) images of metasurfaces fabricated from a-Si [65], c-Si [29], TiO₂ [59], SiN_x [64].

Crystalline silicon (c-Si) has a high refractive index across the NIR, where its indirect bandgap leads to sufficiently low absorption for designing metasurfaces that address Rb and Cs D-line transitions (Fig. 4(a)). The high index and established fabrication techniques from CMOS and silicon photonics make c-Si an attractive material for scalable metasurfaces. c-Si metasurfaces designed for atom trapping have been fabricated starting from silicon-on-insulator [40] and silicon-on-sapphire [29] wafers, with sapphire in particular providing a transparent, chemically inert, and UHV-compatible substrate for integration with cold-atom systems [68]. Amorphous silicon (a-Si) has a narrower region of low losses because structural disorder introduces additional optical loss at most wavelengths [90], though at wavelengths > 800 nm it can be a good option due to its very high index and straightforward growth on transparent substrates via chemical vapor deposition (CVD) [38, 65].

Titanium dioxide (TiO₂) has been extensively used for low-loss visible metasurfaces, including metalenses [84, 85] and reflective metasurfaces for generating colors in visible [91]. TiO₂ combines low absorption with a relatively high refractive index for a low-loss material in the visible ($n \approx 2.4$), enabling, e.g., high-NA metalenses [84]. For neutral-atom systems, this broad transparency range enables the use of metasurfaces to address transitions and trapping wavelengths for, e.g., Yb, Sr, Rb, Cs (Fig. 4(a)). High-quality TiO₂ metasurfaces are typically fabricated either by conformal atomic layer deposition (ALD) filling around a resist mask, followed by planarization [27, 84], or by hard-mask based etching of sputtered TiO₂ films [39]. These approaches can produce high-quality devices, but the former is limited by the slow growth rate of ALD, whereas the latter requires challenging TiO₂ etching [27].

Among the material systems with the lowest losses is silicon nitride (SiN_x). Like Si, this material is CMOS-compatible with available foundry fabrication flows. The refractive index of SiN_x is lower than that of Si but can be adjusted through composition, from stoichiometric Si_3N_4 (with the lowest index; Fig. 4(a)) to silicon-rich nitride [89]. SiN_x metasurfaces have been used as high-NA visible lenses and vortex-beam generators with high transmission [92]. In Ref. [27], a silicon-rich SiN_x metasurface was used to generate Sr tweezer arrays at 520 nm. More broadly, SiN_x is low-loss across visible-to-NIR wavelengths, which are relevant to cooling, imaging, and repumping. Due to the well-established use of SiN_x in photonic integrated circuits [72, 93], it can also be useful for hybrid platforms in which on-chip waveguides deliver and distribute light to integrated metasurfaces for beam shaping, focusing, or trap-array generation.

6 Outlook

We have described the advantages of metasurfaces for generating large numbers of trapping sites and complex trapping profiles, due to the straightforward scalability of metasurface pixel counts into the billions. Metasurfaces have already been used to generate arrays with 360,000 trapping sites [27], far larger than the record number of traps achieved using SLMs [5], and to trap about 11,000 single atoms [30], surpassing the previous record of 6,100 atoms set with SLMs [5]. Looking forward, advanced fabrication processes such as deep-ultraviolet lithography can extend the metasurface pixel counts even more, bringing million-atom arrays into reach.

Beyond advantages in scale, the ability of metasurfaces to imprint nearly arbitrary phase, amplitude, and polarization profiles, combined with dispersion engineering of each meta-atom, enables the combination of multiple functionalities on the same optic. The integration of multiple functionalities can significantly reduce the number of optical components in atomic experiments, enabling robust and portable quantum instruments.

The downside of today’s metasurfaces is that they are not readily tunable, and cannot reproduce the dynamic functionality of SLMs and AODs, for example for rearrangement of atoms or compensating for fluctuations in laser power. It is likely that near-term experiments will combine the unique advantages of metasurfaces with the dynamic tunability of SLMs and AODs, where the active components will be used to fine-tune and reconfigure atomic arrays. Looking further, research into tunable pixel-addressable metasurfaces [94] may integrate the reconfiguration functionality into the metasurfaces themselves.

Funding

This material is based on work supported by the U.S. Department of Energy Office of Science National Quantum Information Science Research Centers, as part of the Q-NEXT center, which is the primary funder. Additional funding support was provided by the National Science Foundation under Award 2016136 for the QLCI center Hybrid Quantum Architectures and Networks, and by the National Science Foundation under Award 2326784 for QuSeC-TAQS.

Disclosures

MS is affiliated with and a shareholder in Inflection, Inc.

Data availability

No original data were generated for this review article.

References

- [1] Adam M. Kaufman and Kang-Kuen Ni. Quantum science with optical tweezer arrays of ultracold atoms and molecules. *Nature Physics*, 17(12):1324–1333, November 2021. ISSN 1745-2481. doi: 10.1038/s41567-021-01357-2. URL <http://doi.org/10.1038/s41567-021-01357-2>.
- [2] F. Nogrette, H. Labuhn, S. Ravets, D. Barredo, L. Béguin, A. Vernier, T. Lahaye, and A. Browaeys. Single-atom trapping in holographic 2D arrays of microtraps with arbitrary geometries. *Physical Review X*, 4(2), May 2014. ISSN 2160-3308. doi: 10.1103/physrevx.4.021034. URL <http://doi.org/10.1103/PhysRevX.4.021034>.
- [3] Hyosub Kim, Woojun Lee, Han-gyeol Lee, Hanlae Jo, Yunheung Song, and Jaewook Ahn. In situ single-atom array synthesis using dynamic holographic optical tweezers. *Nature Communications*, 7(1), October 2016. ISSN 2041-1723. doi: 10.1038/ncomms13317. URL <http://doi.org/10.1038/ncomms13317>.
- [4] Daniel Barredo, Sylvain de Léséleuc, Vincent Lienhard, Thierry Lahaye, and Antoine Browaeys. An atom-by-atom assembler of defect-free arbitrary two-dimensional atomic arrays. *Science*, 354(6315):1021–1023, November 2016. ISSN 1095-9203. doi: 10.1126/science.aah3778. URL <http://doi.org/10.1126/science.aah3778>.
- [5] Hannah J. Manetsch, Gyohei Nomura, Elie Bataille, Xudong Lv, Kon H. Leung, and Manuel Endres. A tweezer array with 6, 100 highly coherent atomic qubits. *Nature*, 647(8088):60–67, 2025. ISSN 1476-4687. doi: 10.1038/s41586-025-09641-4. URL <http://doi.org/10.1038/s41586-025-09641-4>.
- [6] Dustin Stuart and Axel Kuhn. Single-atom trapping and transport in dmd-controlled optical tweezers. *New Journal of Physics*, 20(2):023013, February 2018. ISSN 1367-2630. doi: 10.1088/1367-2630/aaa634. URL <http://doi.org/10.1088/1367-2630/aaa634>.
- [7] Yibo Wang, Sayali Shevate, Tobias Martin Wintermantel, Manuel Morgado, Graham Lockheed, and Shannon Whitlock. Preparation of hundreds of microscopic atomic ensembles in optical tweezer arrays. *npj Quantum Information*, 6(1), 2020. ISSN 2056-6387. doi: 10.1038/s41534-020-0285-1. URL <http://doi.org/10.1038/s41534-020-0285-1>.
- [8] Manuel Endres, Hannes Bernien, Alexander Keesling, Harry Levine, Eric R. Anschuetz, Alexandre Krajenbrink, Crystal Senko, Vladan Vuletic, Markus Greiner, and Mikhail D. Lukin. Atom-by-atom assembly of defect-free one-dimensional cold atom arrays. *Science*, 354(6315):1024–1027, November 2016. ISSN 1095-9203. doi: 10.1126/science.aah3752. URL <http://doi.org/10.1126/science.aah3752>.
- [9] Dolev Bluvstein, Harry Levine, Giulia Semeghini, Tout T. Wang, Sepehr Ebadi, Marcin Kalinowski, Alexander Keesling, Nishad Maskara, Hannes Pichler, Markus Greiner, Vladan Vuletić, and Mikhail D. Lukin. A quantum processor based on coherent transport of entangled atom arrays. *Nature*, 604(7906):451–456, April 2022. ISSN 1476-4687. doi: 10.1038/s41586-022-04592-6. URL <http://doi.org/10.1038/s41586-022-04592-6>.

- [10] Dolev Bluvstein, Simon J. Evered, Alexandra A. Geim, Sophie H. Li, Hengyun Zhou, Tom Manovitz, Sepehr Ebadi, Madelyn Cain, Marcin Kalinowski, Dominik Hangleiter, J. Pablo Bonilla Ataides, Nishad Maskara, Iris Cong, Xun Gao, Pedro Sales Rodriguez, Thomas Karolyshyn, Giulia Semeghini, Michael J. Gullans, Markus Greiner, Vladan Vuletić, and Mikhail D. Lukin. Logical quantum processor based on reconfigurable atom arrays. *Nature*, 626(7997):58–65, 2024. ISSN 1476-4687. doi: 10.1038/s41586-023-06927-3. URL <http://doi.org/10.1038/s41586-023-06927-3>.
- [11] Neng-Chun Chiu, Elias C. Trapp, Jinen Guo, Mohamed H. Abobeih, Luke M. Stewart, Simon Hollerith, Pavel L. Stroganov, Marcin Kalinowski, Alexandra A. Geim, Simon J. Evered, Sophie H. Li, Xingjian Lyu, Lisa M. Peters, Dolev Bluvstein, Tout T. Wang, Markus Greiner, Vladan Vuletić, and Mikhail D. Lukin. Continuous operation of a coherent 3, 000-qubit system. *Nature*, 646(8087):1075–1080, 2025. ISSN 1476-4687. doi: 10.1038/s41586-025-09596-6. URL <http://doi.org/10.1038/s41586-025-09596-6>.
- [12] Kevin Singh, Shraddha Anand, Andrew Pocklington, Jordan T. Kemp, and Hannes Bernien. Dual-element, two-dimensional atom array with continuous-mode operation. *Physical Review X*, 12(1), March 2022. ISSN 2160-3308. doi: 10.1103/physrevx.12.011040. URL <http://doi.org/10.1103/PhysRevX.12.011040>.
- [13] Craig Gidney. How to factor 2048 bit RSA integers with less than a million noisy qubits, 2025. URL <https://arxiv.org/abs/2505.15917>.
- [14] Hengyun Zhou, Casey Duckering, Chen Zhao, Dolev Bluvstein, Madelyn Cain, Aleksander Kubica, Sheng-Tao Wang, and Mikhail D. Lukin. Resource analysis of low-overhead transversal architectures for reconfigurable atom arrays. In *Proceedings of the 52nd Annual International Symposium on Computer Architecture, SIGARCH '25*, page 1432–1448. ACM, 2025. doi: 10.1145/3695053.3731039. URL <http://doi.org/10.1145/3695053.3731039>.
- [15] Joonho Lee, Dominic W. Berry, Craig Gidney, William J. Huggins, Jarrod R. McClean, Nathan Wiebe, and Ryan Babbush. Even more efficient quantum computations of chemistry through tensor hypercontraction. *PRX Quantum*, 2(3), 2021. ISSN 2691-3399. doi: 10.1103/prxquantum.2.030305. URL <http://doi.org/10.1103/PRXQuantum.2.030305>.
- [16] Yuri Alexeev, Maximilian Amsler, Marco Antonio Barroca, Sanzio Bassini, Torey Battelle, Daan Camps, David Casanova, Young Jay Choi, Frederic T Chong, Charles Chung, et al. Quantum-centric supercomputing for materials science: A perspective on challenges and future directions. *Future Generation Computer Systems*, 160:666–710, 2024. doi: 10.1016/j.future.2024.04.060. URL <https://doi.org/10.1016/j.future.2024.04.060>.
- [17] Madelyn Cain, Qian Xu, Robbie King, Lewis R. B. Picard, Harry Levine, Manuel Endres, John Preskill, Hsin-Yuan Huang, and Dolev Bluvstein. Shor’s algorithm is possible with as few as 10,000 reconfigurable atomic qubits, 2026. URL <https://arxiv.org/abs/2603.28627>.
- [18] R. Dumke, M. Volk, T. Mütther, F. B. J. Buchkremer, G. Birkl, and W. Ertmer. Micro-optical realization of arrays of selectively addressable dipole traps: A scalable configuration for quantum computation with atomic qubits. *Physical Review Letters*, 89(9), August 2002. ISSN 1079-7114. doi: 10.1103/physrevlett.89.097903. URL <http://doi.org/10.1103/PhysRevLett.89.097903>.

- [19] Daniel Ohl de Mello, Dominik Schäffner, Jan Werkmann, Tilman Preuschoff, Lars Kohfahl, Malte Schlosser, and Gerhard Birkel. Defect-free assembly of 2D clusters of more than 100 single-atom quantum systems. *Physical Review Letters*, 122(20), May 2019. ISSN 1079-7114. doi: 10.1103/physrevlett.122.203601. URL <http://doi.org/10.1103/PhysRevLett.122.203601>.
- [20] Malte Schlosser, Sascha Tichelmann, Dominik Schäffner, Daniel Ohl de Mello, Moritz Hambach, Jan Schütz, and Gerhard Birkel. Scalable multilayer architecture of assembled single-atom qubit arrays in a three-dimensional Talbot tweezer lattice. *Physical Review Letters*, 130(18), May 2023. ISSN 1079-7114. doi: 10.1103/physrevlett.130.180601. URL <http://doi.org/10.1103/PhysRevLett.130.180601>.
- [21] Lars Pause, Tilman Preuschoff, Dominik Schäffner, Malte Schlosser, and Gerhard Birkel. Reservoir-based deterministic loading of single-atom tweezer arrays. *Physical Review Research*, 5(3), 2023. ISSN 2643-1564. doi: 10.1103/physrevresearch.5.l032009. URL <http://doi.org/10.1103/PhysRevResearch.5.L032009>.
- [22] Lars Pause, Lukas Sturm, Marcel Mittenbühler, Stephan Amann, Tilman Preuschoff, Dominik Schäffner, Malte Schlosser, and Gerhard Birkel. Supercharged two-dimensional tweezer array with more than 1000 atomic qubits. *Optica*, 11(2):222, February 2024. ISSN 2334-2536. doi: 10.1364/optica.513551. URL <http://doi.org/10.1364/OPTICA.513551>.
- [23] P. Huft, Y. Song, T. M. Graham, K. Jooya, S. Deshpande, C. Fang, M. Kats, and M. Saffman. Simple, passive design for large optical trap arrays for single atoms. *Physical Review A*, 105(6), 2022. ISSN 2469-9934. doi: 10.1103/physreva.105.063111. URL <http://doi.org/10.1103/PhysRevA.105.063111>.
- [24] Chengyu Fang, Jared Miles, Jonathan Goldwin, Martin Lichtman, Matthew Gillette, Michael Bergdolt, Sanket Deshpande, Sam A. Norrell, Preston Huft, Mikhail A. Kats, and Mark Saffman. Interleaved dual-species arrays of single atoms using a passive optical element and one trapping laser. *Science Advances*, 11(29), 2025. ISSN 2375-2548. doi: 10.1126/sciadv.adw4166. URL <http://doi.org/10.1126/sciadv.adw4166>.
- [25] Nanfang Yu, Patrice Genevet, Mikhail A. Kats, Francesco Aieta, Jean-Philippe Tetienne, Federico Capasso, and Zeno Gaburro. Light propagation with phase discontinuities: Generalized laws of reflection and refraction. *Science*, 334(6054):333–337, October 2011. ISSN 1095-9203. doi: 10.1126/science.1210713. URL <http://doi.org/10.1126/science.1210713>.
- [26] M. Saffman, T. G. Walker, and K. Mølmer. Quantum information with Rydberg atoms. *Reviews of Modern Physics*, 82(3):2313–2363, August 2010. ISSN 1539-0756. doi: 10.1103/revmodphys.82.2313. URL <http://doi.org/10.1103/RevModPhys.82.2313>.
- [27] Aaron Holman, Yuan Xu, Ximo Sun, Jiahao Wu, Mingxuan Wang, Zezheng Zhu, Bojeong Seo, Nanfang Yu, and Sebastian Will. Trapping of single atoms in metasurface optical tweezer arrays. *Nature*, 649(8098):859–865, January 2026. ISSN 1476-4687. doi: 10.1038/s41586-025-09961-5. URL <http://doi.org/10.1038/s41586-025-09961-5>.
- [28] Yuqing Wang, Yuxuan Liao, Tao Zhang, Ye Tian, Yujia Wu, Wenjun Zhang, Wei Zhang, Yidong Huang, Hui Zhai, Wenlan Chen, Xue Feng, and Zhongchi Zhang. Direct generation of an array with 78400 optical tweezers using a single metasurface. *Chinese Physics Letters*, 43(1):010606, December 2025. ISSN 1741-3540. doi: 10.1088/0256-307x/43/1/010606. URL <http://doi.org/10.1088/0256-307X/43/1/010606>.

- [29] Chengyu Fang, Minjeong Kim, Hongyan Mei, Xuting Yang, Zhaoning Yu, Yuzhe Xiao, Sanket Deshpande, Preston Huft, Alan M. Dibos, David A. Czaplewski, Mark Saffman, Jennifer T. Choy, and Mikhail A. Kats. Silicon-on-sapphire metasurfaces generate arrays of dark and bright traps for neutral atoms, 2026. URL <https://arxiv.org/abs/2601.01038>.
- [30] Yuqing Wang, Zhongchi Zhang, Tao Zhang, Yuxuan Liao, Hanteng Wang, Ye Tian, Binjie Ji, Yujia Wu, Luming Ma, Chen Qing, Chengshu Li, Wei Zhang, Yidong Huang, Wenjun Zhang, Xue Feng, Wenlan Chen, and Hui Zhai. Trapping 11,000 atoms in a tweezer array generated by a single metasurface, 2026. URL <https://arxiv.org/abs/2606.02715>.
- [31] Ralph W Gerchberg and W Owen Saxton. A practical algorithm for the determination of the phase from image and diffraction plane pictures. *Optik*, 35(2):237–246, 1972.
- [32] Shaohua Tao and Weixing Yu. Beam shaping of complex amplitude with separate constraints on the output beam. *Optics Express*, 23(2):1052, January 2015. ISSN 1094-4087. doi: 10.1364/oe.23.001052. URL <http://doi.org/10.1364/OE.23.001052>.
- [33] Keisuke Nishimura, Hiroto Sakai, Taro Ando, Takafumi Tomita, and Sylvain de Léséleuc. Optimization-based hologram design for fine optical tweezer arrays and extension of super-resolution criteria. *Physical Review A*, 113(1), January 2026. ISSN 2469-9934. doi: 10.1103/xhb8-jlxh. URL <http://doi.org/10.1103/xhb8-jlxh>.
- [34] Rui Lin, Han-Sen Zhong, You Li, Zhang-Rui Zhao, Le-Tian Zheng, Tai-Ran Hu, Hong-Ming Wu, Zhan Wu, Wei-Jie Ma, Yan Gao, Yi-Kang Zhu, Zhao-Feng Su, Wan-Li Ouyang, Yu-Chen Zhang, Jun Rui, Ming-Cheng Chen, Chao-Yang Lu, and Jian-Wei Pan. AI-enabled parallel assembly of thousands of defect-free neutral atom arrays. *Physical Review Letters*, 135(6), August 2025. ISSN 1079-7114. doi: 10.1103/2ym8-vs82. URL <http://doi.org/10.1103/2ym8-vs82>.
- [35] Kun Wang, Xiao-Feng Liu, Yuan-An Zhao, Chun-Xian Tao, Jian-Guo Wang, Shao-Zhong Ou, Zhi-Chang Mo, Zhao-Liang Cao, Da-Wei Li, Da-Wei Zhang, and Jian-Da Shao. Phase degradation of liquid crystal variable retarders and preconfiguring method for high-power continuous-wave laser. *Optical Materials*, 141:113920, 2023. ISSN 0925-3467. doi: 10.1016/j.optmat.2023.113920. URL <http://doi.org/10.1016/j.optmat.2023.113920>.
- [36] Philip Zupancic, Philipp M. Preiss, Ruichao Ma, Alexander Lukin, M. Eric Tai, Matthew Rispoli, Rajibul Islam, and Markus Greiner. Ultra-precise holographic beam shaping for microscopic quantum control. *Optics Express*, 24(13):13881, 2016. ISSN 1094-4087. doi: 10.1364/oe.24.013881. URL <http://doi.org/10.1364/OE.24.013881>.
- [37] Y. T. Chew, M. Poittrinal, T. Tomita, S. Kitade, J. Mauricio, K. Ohmori, and S. de Léséleuc. Ultraprecise holographic optical tweezer array. *Physical Review A*, 110(5), November 2024. ISSN 2469-9934. doi: 10.1103/physreva.110.053518. URL <http://doi.org/10.1103/PhysRevA.110.053518>.
- [38] T.-W. Hsu, W. Zhu, T. Thiele, M. O. Brown, S. B. Papp, A. Agrawal, and C. A. Regal. Single-atom trapping in a metasurface-lens optical tweezer. *PRX Quantum*, 3(3), August 2022. ISSN 2691-3399. doi: 10.1103/prxquantum.3.030316. URL <http://doi.org/10.1103/PRXQuantum.3.030316>.

- [39] Xiaoyan Huang, Weijun Yuan, Aaron Holman, Minho Kwon, Stuart J. Masson, Ricardo Gutierrez-Jauregui, Ana Asenjo-Garcia, Sebastian Will, and Nanfang Yu. Metasurface holographic optical traps for ultracold atoms. *Progress in Quantum Electronics*, 89:100470, May 2023. ISSN 0079-6727. doi: 10.1016/j.pquantelec.2023.100470. URL <http://doi.org/10.1016/j.pquantelec.2023.100470>.
- [40] Ruiting Huang, Feng Zhou, Xiao Li, Peng Xu, Yi Wang, and Mingsheng Zhan. Metasurface optical trap array for single atoms. *Optics Express*, 32(12):21293, May 2024. ISSN 1094-4087. doi: 10.1364/oe.525454. URL <http://doi.org/10.1364/OE.525454>.
- [41] Joon-Suh Park, Soon Wei Daniel Lim, Arman Amirzhan, Hyukmo Kang, Karlene Karrfalt, Daewook Kim, Joel Leger, Augustine Urbas, Marcus Ossiander, Zhaoyi Li, and Federico Capasso. All-glass 100 mm diameter visible metalens for imaging the cosmos. *ACS Nano*, 18(4):3187–3198, January 2024. ISSN 1936-086X. doi: 10.1021/acsnano.3c09462. URL <http://doi.org/10.1021/acsnano.3c09462>.
- [42] Dong Kyo Oh, Taejun Lee, Byoungsu Ko, Trevon Badloe, Jong G. Ok, and Junsuk Rho. Nanoimprint lithography for high-throughput fabrication of metasurfaces. *Frontiers of Optoelectronics*, 14(2):229–251, April 2021. ISSN 2095-2767. doi: 10.1007/s12200-021-1121-8. URL <http://doi.org/10.1007/s12200-021-1121-8>.
- [43] Matthew Pasienski and Brian DeMarco. A high-accuracy algorithm for designing arbitrary holographic atom traps. *Optics Express*, 16(3):2176, 2008. ISSN 1094-4087. doi: 10.1364/oe.16.002176. URL <http://doi.org/10.1364/OE.16.002176>.
- [44] G. Li, S. Zhang, L. Isenhower, K. Maller, and M. Saffman. Crossed vortex bottle beam trap for single-atom qubits. *Optics Letters*, 37(5):851, February 2012. ISSN 1539-4794. doi: 10.1364/ol.37.000851. URL <http://doi.org/10.1364/OL.37.000851>.
- [45] Roez Ozeri, Lev Khaykovich, and Nir Davidson. Long spin relaxation times in a single-beam blue-detuned optical trap. *Physical Review A*, 59(3):R1750–R1753, March 1999. ISSN 1094-1622. doi: 10.1103/physreva.59.r1750. URL <http://doi.org/10.1103/PhysRevA.59.R1750>.
- [46] S. Kuhr, W. Alt, D. Schrader, I. Dotsenko, Y. Miroshnychenko, A. Rauschenbeutel, and D. Meschede. Analysis of dephasing mechanisms in a standing-wave dipole trap. *Physical Review A*, 72(2), August 2005. ISSN 1094-1622. doi: 10.1103/physreva.72.023406. URL <http://doi.org/10.1103/PhysRevA.72.023406>.
- [47] Rudolf Grimm, Matthias Weidemüller, and Yurii B. Ovchinnikov. *Optical Dipole Traps for Neutral Atoms*, page 95–170. Elsevier, 2000. ISBN 9780120038428. doi: 10.1016/S1049-250X(08)60186-X. URL [http://doi.org/10.1016/S1049-250X\(08\)60186-X](http://doi.org/10.1016/S1049-250X(08)60186-X).
- [48] M. Saffman and T. G. Walker. Analysis of a quantum logic device based on dipole-dipole interactions of optically trapped Rydberg atoms. *Physical Review A*, 72(2), August 2005. ISSN 1094-1622. doi: 10.1103/physreva.72.022347. URL <http://doi.org/10.1103/PhysRevA.72.022347>.
- [49] Lukas Ahlheit, Chris Nill, Daniil Svirskiy, Jan de Haan, Simon Schroers, Wolfgang Alt, Nina Stiesdal, Igor Lesanovsky, and Sebastian Hofferberth. Magic running- and standing-wave optical traps for Rydberg atoms. *Physical Review A*, 111(1), January 2025. ISSN 2469-9934. doi: 10.1103/physreva.111.013115. URL <http://doi.org/10.1103/PhysRevA.111.013115>.

- [50] Hannes Bernien, Sylvain Schwartz, Alexander Keesling, Harry Levine, Ahmed Omran, Hannes Pichler, Soonwon Choi, Alexander S. Zibrov, Manuel Endres, Markus Greiner, Vladan Vuletić, and Mikhail D. Lukin. Probing many-body dynamics on a 51-atom quantum simulator. *Nature*, 551(7682):579–584, November 2017. ISSN 1476-4687. doi: 10.1038/nature24622. URL <http://doi.org/10.1038/nature24622>.
- [51] T. Wilk, A. Gaëtan, C. Evellin, J. Wolters, Y. Miroshnychenko, P. Grangier, and A. Browaeys. Entanglement of two individual neutral atoms using Rydberg blockade. *Physical Review Letters*, 104(1), January 2010. ISSN 1079-7114. doi: 10.1103/physrevlett.104.010502. URL <http://doi.org/10.1103/PhysRevLett.104.010502>.
- [52] Nikolaus Lorenz, Lorenzo Festa, Lea-Marina Steinert, and Christian Gross. Raman side-band cooling in optical tweezer arrays for Rydberg dressing. *SciPost Physics*, 10(3), March 2021. ISSN 2542-4653. doi: 10.21468/scipostphys.10.3.052. URL <http://doi.org/10.21468/SciPostPhys.10.3.052>.
- [53] R. J. P. T. de Keijzer, O. Tse, and S. J. J. M. F. Kokkelmans. Recapture probability for antitrapped Rydberg states in optical tweezers. *Physical Review A*, 108(2), August 2023. ISSN 2469-9934. doi: 10.1103/physreva.108.023122. URL <http://doi.org/10.1103/PhysRevA.108.023122>.
- [54] D. Barredo, V. Lienhard, P. Scholl, S. de Léséleuc, T. Boulier, A. Browaeys, and T. Lahaye. Three-dimensional trapping of individual Rydberg atoms in ponderomotive bottle beam traps. *Physical Review Letters*, 124(2), January 2020. ISSN 1079-7114. doi: 10.1103/physrevlett.124.023201. URL <http://doi.org/10.1103/PhysRevLett.124.023201>.
- [55] S. Zhang, F. Robicheaux, and M. Saffman. Magic-wavelength optical traps for Rydberg atoms. *Physical Review A*, 84(4), October 2011. ISSN 1094-1622. doi: 10.1103/physreva.84.043408. URL <http://doi.org/10.1103/PhysRevA.84.043408>.
- [56] L. Isenhower, W. Williams, A. Dally, and M. Saffman. Atom trapping in an interferometrically generated bottle beam trap. *Optics Letters*, 34(8):1159, April 2009. ISSN 1539-4794. doi: 10.1364/ol.34.001159. URL <http://doi.org/10.1364/OL.34.001159>.
- [57] Yuzhe Xiao, Zhaoning Yu, Raymond A. Wambold, Hongyan Mei, Garrett Hickman, Randall H. Goldsmith, Mark Saffman, and Mikhail A. Kats. Efficient generation of optical bottle beams. *Nanophotonics*, 10(11):2893–2901, 2021. ISSN 2192-8614. doi: 10.1515/nanoph-2021-0243. URL <http://doi.org/10.1515/nanoph-2021-0243>.
- [58] Kaixiang Cheng, Yan Li, Yi Liu, Yanhua Han, Xiaosai Wang, Jianwen Wu, and Yaqi Zhang. Generation of vectorial structured light carrying bright and dark focus for multifunctional optical trapping via spin-decoupled metasurfaces. *Optics Letters*, 50(21):6847, October 2025. ISSN 1539-4794. doi: 10.1364/ol.573997. URL <http://doi.org/10.1364/OL.573997>.
- [59] Soon Wei Daniel Lim, Joon-Suh Park, Dmitry Kazakov, Christina M. Spägle, Ahmed H. Dorrah, Maryna L. Meretska, and Federico Capasso. Point singularity array with metasurfaces. *Nature Communications*, 14(1), 2023. ISSN 2041-1723. doi: 10.1038/s41467-023-39072-6. URL <http://doi.org/10.1038/s41467-023-39072-6>.
- [60] K. Singh, C. E. Bradley, S. Anand, V. Ramesh, R. White, and H. Bernien. Mid-circuit correction of correlated phase errors using an array of spectator qubits. *Science*, 380(6651):

- 1265–1269, 2023. ISSN 1095-9203. doi: 10.1126/science.ade5337. URL <http://doi.org/10.1126/science.ade5337>.
- [61] D. Petrosyan, S. Norrell, C. Poole, and M. Saffman. Fast measurements and multiqubit gates in dual-species atomic arrays. *Physical Review A*, 110(4), October 2024. ISSN 2469-9934. doi: 10.1103/physreva.110.042404. URL <http://doi.org/10.1103/PhysRevA.110.042404>.
- [62] Shaokang Li, Gang Li, Wei Wu, Qing Fan, Yali Tian, Pengfei Yang, Pengfei Zhang, and Tiancai Zhang. High-numerical-aperture and long-working-distance objective for single-atom experiments. *Review of Scientific Instruments*, 91(4), April 2020. ISSN 1089-7623. doi: 10.1063/5.0001637. URL <http://doi.org/10.1063/5.0001637>.
- [63] E. L. Raab, M. Prentiss, Alex Cable, Steven Chu, and D. E. Pritchard. Trapping of neutral sodium atoms with radiation pressure. *Physical Review Letters*, 59(23):2631–2634, December 1987. ISSN 0031-9007. doi: 10.1103/physrevlett.59.2631. URL <http://doi.org/10.1103/PhysRevLett.59.2631>.
- [64] Mingke Jin, Xu Zhang, Xuan Liu, Changwen Liang, Jixun Liu, Zixian Hu, Kingfai Li, Guochao Wang, Jun Yang, Lingxiao Zhu, and Guixin Li. A centimeter-scale dielectric metasurface for the generation of cold atoms. *Nano Letters*, 23(9):4008–4013, April 2023. ISSN 1530-6992. doi: 10.1021/acs.nanolett.3c00791. URL <http://doi.org/10.1021/acs.nanolett.3c00791>.
- [65] Tian Tian, Chen Qing, Yuxuan Liao, Jiajun Zhu, Yongzhuo Li, Xue Feng, Dengke Zhang, and Yidong Huang. Polarization decoupling multi-port beam-splitting metasurface for miniaturized magneto-optical trap. *Advanced Science*, 12(37), 2025. ISSN 2198-3844. doi: 10.1002/advs.202506289. URL <http://doi.org/10.1002/advs.202506289>.
- [66] Guang-Jie Chen, Dong Zhao, Zhu-Bo Wang, Ziqin Li, Ji-Zhe Zhang, Liang Chen, Yan-Lei Zhang, Xin-Biao Xu, Ai-Ping Liu, Chun-Hua Dong, Guang-Can Guo, Kun Huang, and Chang-Ling Zou. Multifunctional metalens for trapping and characterizing single atoms. *Laser & Photonics Reviews*, 19(6), December 2024. ISSN 1863-8899. doi: 10.1002/lpor.202401595. URL <http://doi.org/10.1002/lpor.202401595>.
- [67] Chad Ropp, Wenqi Zhu, Alexander Yulaev, Daron Westly, Gregory Simelgor, Akash Rakholia, William Lunden, Dan Sheredy, Martin M. Boyd, Scott Papp, Amit Agrawal, and Vladimir Aksyuk. Integrating planar photonics for multi-beam generation and atomic clock packaging on chip. *Light: Science & Applications*, 12(1), April 2023. ISSN 2047-7538. doi: 10.1038/s41377-023-01081-x. URL <http://doi.org/10.1038/s41377-023-01081-x>.
- [68] Xuting Yang, Pritha Mukherjee, Minjeong Kim, Hongyan Mei, Chengyu Fang, Soyeon Choi, Yuhan Tong, Sarah Perlowski, David A. Czaplewski, Alan M. Dibos, Mikhail A. Kats, and Jennifer T. Choy. Atomic magnetometry using a metasurface polarizing beamsplitter in silicon-on-sapphire. *ACS Photonics*, 11(9):3644–3651, 2024. ISSN 2330-4022. doi: 10.1021/acsp Photonics.4c00744. URL <http://doi.org/10.1021/acsp Photonics.4c00744>.
- [69] Wei Ting Chen, Alexander Y. Zhu, Vyshakh Sanjeev, Mohammadreza Khorasaninejad, Zhujun Shi, Eric Lee, and Federico Capasso. A broadband achromatic metalens for focusing and imaging in the visible. *Nature Nanotechnology*, 13(3):220–226, January 2018. ISSN 1748-3395. doi: 10.1038/s41565-017-0034-6. URL <http://doi.org/10.1038/s41565-017-0034-6>.

- [70] J. D. Pritchard, J. A. Isaacs, and M. Saffman. Long working distance objective lenses for single atom trapping and imaging. *Review of Scientific Instruments*, 87(7), 2016. ISSN 1089-7623. doi: 10.1063/1.4959775. URL <http://doi.org/10.1063/1.4959775>.
- [71] Kunhong Shen, Yao Duan, Peng Ju, Zhuqing Xu, Xi Chen, Lidan Zhang, Jonghoon Ahn, Xingjie Ni, and Tongcang Li. On-chip optical levitation with a metalens in vacuum. *Optica*, 8(11):1359, October 2021. ISSN 2334-2536. doi: 10.1364/optica.438410. URL <http://doi.org/10.1364/OPTICA.438410>.
- [72] Andrei Isichenko, Nitesh Chauhan, Debapam Bose, Jiawei Wang, Paul D. Kunz, and Daniel J. Blumenthal. Photonic integrated beam delivery for a rubidium 3D magneto-optical trap. *Nature Communications*, 14(1), May 2023. ISSN 2041-1723. doi: 10.1038/s41467-023-38818-6. URL <http://doi.org/10.1038/s41467-023-38818-6>.
- [73] Daniel J. Blumenthal, Andrei Isichenko, and Nitesh Chauhan. Enabling photonic integrated 3D magneto-optical traps for quantum sciences and applications. *Optica Quantum*, 2(6):444, December 2024. ISSN 2837-6714. doi: 10.1364/opticaq.532260. URL <http://doi.org/10.1364/OPTICAQ.532260>.
- [74] Sindhu Jammi, Andrew R. Ferdinand, Zheng Luo, Zachary L. Newman, Grisha Spektor, Junyeob Song, Okan Koksals, Akash V. Rakholia, William Lunden, Daniel Sheredy, Parth B. Patel, Martin M. Boyd, Wenqi Zhu, Amit Agrawal, Travis C. Briles, and Scott B. Papp. Three-dimensional, multi-wavelength beam formation with integrated metasurface optics for sr laser cooling. *Optics Letters*, 49(21):6013, October 2024. ISSN 1539-4794. doi: 10.1364/ol.526056. URL <http://doi.org/10.1364/OL.526056>.
- [75] Andrew R. Ferdinand, Zheng Luo, Sindhu Jammi, Zachary Newman, Grisha Spektor, Okan Koksals, Parth B. Patel, Daniel Sheredy, William Lunden, Akash Rakholia, Travis C. Briles, Wenqi Zhu, Martin M. Boyd, Amit Agrawal, and Scott B. Papp. Laser-cooling ^{88}Sr to microkelvin temperature with an integrated-photonics system. *Physical Review Applied*, 23(3), March 2025. ISSN 2331-7019. doi: 10.1103/physrevapplied.23.l031002. URL <http://doi.org/10.1103/PhysRevApplied.23.L031002>.
- [76] Zheng Luo, Travis C. Briles, Zachary L. Newman, Aidan R. Jones, Andrew R. Ferdinand, Sindhu Jammi, Grisha Spektor, David R. Carlson, Akash Rakholia, Dan Sheredy, Parth Patel, Martin M. Boyd, Chad Ropp, Daron Westly, Vladimir A. Aksyuk, Wenqi Zhu, Junyeob Song, Amit Agrawal, and Scott B. Papp. A scalable infrastructure for strontium optical clocks with integrated photonics, 2026. URL <https://arxiv.org/abs/2604.03229>.
- [77] Vishal Shah, Svenja Knappe, Peter D. D. Schwindt, and John Kitching. Subpicotesla atomic magnetometry with a microfabricated vapour cell. *Nature Photonics*, 1(11):649–652, November 2007. ISSN 1749-4893. doi: 10.1038/nphoton.2007.201. URL <http://doi.org/10.1038/nphoton.2007.201>.
- [78] Dmitry Budker and Michael Romalis. Optical magnetometry. *Nature Physics*, 3(4):227–234, April 2007. ISSN 1745-2481. doi: 10.1038/nphys566. URL <http://doi.org/10.1038/nphys566>.
- [79] John Kitching. Chip-scale atomic devices. *Applied Physics Reviews*, 5(3):031302, 2018. ISSN 1931-9401. doi: 10.1063/1.5026238. URL <http://doi.org/10.1063/1.5026238>.

- [80] Yoel Sebbag, Alex Naiman, Eliran Talker, Yefim Barash, and Uriel Levy. Chip-scale integration of nanophotonic-atomic magnetic sensors. *ACS Photonics*, 8(1):142–146, December 2020. ISSN 2330-4022. doi: 10.1021/acsp Photonics.0c01473. URL <http://doi.org/10.1021/acsp Photonics.0c01473>.
- [81] Yoel Sebbag, Eliran Talker, Alex Naiman, Yefim Barash, and Uriel Levy. Demonstration of an integrated nanophotonic chip-scale alkali vapor magnetometer using inverse design. *Light: Science & Applications*, 10(1), March 2021. ISSN 2047-7538. doi: 10.1038/s41377-021-00499-5. URL <http://doi.org/10.1038/s41377-021-00499-5>.
- [82] Robert C. Devlin, Mohammadreza Khorasaninejad, Wei Ting Chen, Jaewon Oh, and Federico Capasso. Broadband high-efficiency dielectric metasurfaces for the visible spectrum. *Proceedings of the National Academy of Sciences*, 113(38):10473–10478, 2016. ISSN 1091-6490. doi: 10.1073/pnas.1611740113. URL <http://doi.org/10.1073/pnas.1611740113>.
- [83] T. S. Moss. Relations between the refractive index and energy gap of semiconductors. *physica status solidi (b)*, 131(2):415–427, October 1985. ISSN 1521-3951. doi: 10.1002/pssb.2221310202. URL <http://doi.org/10.1002/pssb.2221310202>.
- [84] Mohammadreza Khorasaninejad, Wei Ting Chen, Robert C. Devlin, Jaewon Oh, Alexander Y. Zhu, and Federico Capasso. Metalenses at visible wavelengths: Diffraction-limited focusing and subwavelength resolution imaging. *Science*, 352(6290):1190–1194, 2016. ISSN 1095-9203. doi: 10.1126/science.aaf6644. URL <http://doi.org/10.1126/science.aaf6644>.
- [85] Yaoyao Liang, Hongzhan Liu, Faqiang Wang, Hongyun Meng, Jianping Guo, Jinfeng Li, and Zhongchao Wei. High-efficiency, near-diffraction limited, dielectric metasurface lenses based on crystalline titanium dioxide at visible wavelengths. *Nanomaterials*, 8(5):288, April 2018. ISSN 2079-4991. doi: 10.3390/nano8050288. URL <http://doi.org/10.3390/nano8050288>.
- [86] David Sell, Jianji Yang, Sage Doshay, Kai Zhang, and Jonathan A. Fan. Visible light metasurfaces based on single-crystal silicon. *ACS Photonics*, 3(10):1919–1925, October 2016. ISSN 2330-4022. doi: 10.1021/acsp Photonics.6b00436. URL <http://doi.org/10.1021/acsp Photonics.6b00436>.
- [87] Zhenpeng Zhou, Juntao Li, Rongbin Su, Beimeng Yao, Hanlin Fang, Kezheng Li, Lidan Zhou, Jin Liu, Daan Stellinga, Christopher P. Reardon, Thomas F. Krauss, and Xuehua Wang. Efficient silicon metasurfaces for visible light. *ACS Photonics*, 4(3):544–551, February 2017. ISSN 2330-4022. doi: 10.1021/acsp Photonics.6b00740. URL <http://doi.org/10.1021/acsp Photonics.6b00740>.
- [88] Omer Can Karaman, Gopal Narmada Naidu, Alan R. Bowman, Elif Nur Dayi, and Giulia Tagliabue. Decoupling optical and thermal dynamics in dielectric metasurfaces for self-encoded photonic control. *Laser & Photonics Reviews*, 19(24), August 2025. ISSN 1863-8899. doi: 10.1002/lpor.202501014. URL <http://doi.org/10.1002/lpor.202501014>.
- [89] Tanuj Kumar, Demeng Feng, Shenwei Yin, Merlin Mah, Phyo Lin, Margaret A. Fortman, Gabriel R. Jaffe, Chenghao Wan, Hongyan Mei, Yuzhe Xiao, Ron Synowicki, Ronald J. Warzoha, Victor W. Brar, Joseph J. Talghader, and Mikhail A. Kats. Self-referencing photothermal common-path interferometry to measure absorption of Si₃N₄ membranes for laser-light sails. *ACS Photonics*, 12(11):6381–6387, October 2025. ISSN 2330-4022. doi: 10.1021/acsp Photonics.5c01886. URL <http://doi.org/10.1021/acsp Photonics.5c01886>.

- [90] G. D. Cody, T. Tiedje, B. Abeles, B. Brooks, and Y. Goldstein. Disorder and the optical-absorption edge of hydrogenated amorphous silicon. *Physical Review Letters*, 47(20):1480–1483, November 1981. ISSN 0031-9007. doi: 10.1103/physrevlett.47.1480. URL <http://doi.org/10.1103/PhysRevLett.47.1480>.
- [91] Shang Sun, Zhenxing Zhou, Chen Zhang, Yisheng Gao, Zonghui Duan, Shumin Xiao, and Qinghai Song. All-dielectric full-color printing with TiO₂ metasurfaces. *ACS Nano*, 11(5):4445–4452, March 2017. ISSN 1936-086X. doi: 10.1021/acsnano.7b00415. URL <http://doi.org/10.1021/acsnano.7b00415>.
- [92] Alan Zhan, Shane Colburn, Rahul Trivedi, Taylor K. Fryett, Christopher M. Dodson, and Arka Majumdar. Low-contrast dielectric metasurface optics. *ACS Photonics*, 3(2):209–214, February 2016. ISSN 2330-4022. doi: 10.1021/acsp Photonics.5b00660. URL <http://doi.org/10.1021/acsp Photonics.5b00660>.
- [93] Shankar G. Menon, Noah Glachman, Matteo Pompili, Alan Dibos, and Hannes Bernien. An integrated atom array-nanophotonic chip platform with background-free imaging. *Nature Communications*, 15(1), 2024. ISSN 2041-1723. doi: 10.1038/s41467-024-50355-4. URL <http://doi.org/10.1038/s41467-024-50355-4>.
- [94] Omar A. M. Abdelraouf, Ziyu Wang, Hailong Liu, Zhaogang Dong, Qian Wang, Ming Ye, Xiao Renshaw Wang, Qi Jie Wang, and Hong Liu. Recent advances in tunable metasurfaces: Materials, design, and applications. *ACS Nano*, 16(9):13339–13369, August 2022. ISSN 1936-086X. doi: 10.1021/acsnano.2c04628. URL <http://doi.org/10.1021/acsnano.2c04628>.